

# The Extended Solar Cycle Tracked High into the Corona.

S.J. Tappin\*, R.C. Altrock†

September 14, 2012

## Abstract

We present observations of the extended solar cycle activity in white-light coronagraphs, and compare them with the more familiar features seen in the Fe XIV green-line corona. We show that the coronal activity zones seen in the emission corona can be tracked high into the corona. The peak latitude of the activity, which occurs near solar maximum, is found to be very similar at all heights. But we find that the equatorward drift of the activity zones is faster at greater heights, and that during the declining phase of the solar cycle, the lower branch of activity (that associated with the current cycle) disappears at about  $3R_{\odot}$ . This implies that during the declining phase of the cycle, the solar wind detected near Earth is likely to be dominated by the next cycle. The so-called “rush to the poles” is also seen in the higher corona. In the higher corona it is found to start at a similar time but at lower latitudes than in the green-line corona. The structure is found to be similar to that of the equatorward drift.

## 1 Introduction

The existence of an “extended solar cycle” in which features related to the next cycle appear at high latitudes around or soon after the maximum of the current cycle has been known on the solar surface and in the low corona for many years (*e.g.* Labonte and Howard, 1982; Wilson et al., 1988; Altrock, 1997). Typically this activity is observed in the form of ephemeral active regions, torsional waves and coronal streamers observed in the Fe XIV green line. Having appeared near solar maximum, these structures then drift equatorwards mirroring the “butterfly” pattern of sunspots and active regions at lower latitudes in the current cycle. Following solar minimum, the sunspots and active regions reappear at the same latitudes as this descending coronal and rotational structure. At this time a zone of coronal activity detaches from the main zone and moves rapidly poleward, joining the next extended cycle around solar maximum, this is described as the “rush to the poles” (Waldemeier, 1964), (see also Altrock (2011) for examples).

---

\*National Solar Observatory, Sacramento Peak, Sunspot, NM, USA, email: jtappin@nso.edu

†Air Force Research Laboratory, Space Weather Center of Excellence, National Solar Observatory, Sacramento Peak, Sunspot, NM, USA, email: altrock@nso.edu

To date, studies of the extended cycle and of the rush to the poles have been confined to the solar surface and the low corona. But now that observations from the LASCO coronagraphs on SOHO (Brueckner *et al.*, 1995) are available for more than a complete solar cycle it is possible to carry out an investigation of how these structures propagate into the higher corona.

In this paper we combine the Fe XIV green-line and white-light coronagraph observations to trace the evolution of the zones of activity in latitude as a function of height above the solar limb and phase of the solar cycle.

## 2 The Observations

In this paper we make use of five coronagraph datasets to track activity in the corona from  $1.15R_{\odot}$  to  $20R_{\odot}$  (N.B. in this paper, all heights are measured from Sun centre).

### 2.1 NSO Green Line

The Fe XIV 530.3 nm green line coronagraph observations made at the National Solar Observatory at Sacramento Peak (NSO/SP), have been discussed in some detail by Altrock (1997). In this study we have used those data from 1986 to the end of 2011. In summary: On each day with sufficiently good observing conditions a scan of the corona is made at a distance of  $1.15R_{\odot}$  from disk centre with an angular resolution of  $3^{\circ}$  in position angle, and a scan width of 1.1 arcmin.

### 2.2 MLSO Polarised White Light (Mk3 and Mk4 Coronameters)

The Mauna Loa Solar Observatory (MLSO) has been making white-light polarised brightness images since 1980. The Mk3 coronameter (Fisher *et al.*, 1981) was operated from 1980 to 1999, and the Mk4 (Elmore *et al.*, 2003) from 1998 to the present. For both instruments a linear detector array is scanned around the corona to build up an image in position angle and radial distance. For the Mk3 instrument a few scans were made each day (during the interval considered in this paper there are typically two or three images on the MLSO data download site) while for the Mk4 scans are taken every three minutes through the 5-h observing day. These scans are published at an angular resolution of  $0.5^{\circ}$  in position angle by 10 arcsec in the radial direction for Mk3, and 5 arcsec for Mk4. Both instruments cover similar regions of the corona,  $1.12R_{\odot}$  to  $2.44R_{\odot}$  for Mk3 and  $1.12R_{\odot}$  to  $2.86R_{\odot}$  for Mk4. For this study we have used the daily average images for all available days from 1986 to 2011 (for 2009 and 2010, where many daily average images are missing, we have downloaded the full dataset and generated daily average images from the individual scans). During the interval of overlap we use the Mk4 image if both are available. At the time of writing the most recent data available were for 19 September 2011.

Observatory	Heights
NSO/SP	<b>1.15</b>
MLSO (both)	<b>1.15</b> , 1.20, 1.25, 1.30, <b>1.4</b> , 1.5, 1.6, <b>1.7</b> , 1.8, 1.9, <b>2.0</b> , 2.2, <b>2.35</b>
LASCO (C2)	<b>2.5</b> , 2.75, <b>3.0</b> , 3.25, <b>3.5</b> , 3.75, <b>4.0</b>
LASCO (C3)	5.0, <b>6.0</b> , 7.0, 8.0, 9.0, <b>10.0</b> , 12.0, <b>14.0</b> , 16.0, 18.0, <b>20.0</b>

Table 1: The heights of the scans used in this study. All distances are in units of  $R_{\odot}$  from the centre of the Sun. The heights which are shown in Figure 2 are indicated by **bold** font.

### 2.3 LASCO White Light (C2 and C3)

The LASCO coronagraphs on SOHO (Brueckner *et al.*, 1995), have been making regular images of the corona since late 1995. For this study we use the C2 coronagraph which covers the range from about  $2R_{\odot}$  to  $6R_{\odot}$ , and the C3 coronagraph which covers the range from about  $4R_{\odot}$  to  $30R_{\odot}$ . For C2 the images are taken using an orange filter with a cadence of about 20 min for most of the mission. C3 has a cadence of around 30 min and uses a clear filter for its primary synoptic sequence. At the time of writing the most recent data available were for 1 April 2011.

## 3 Data Processing

The first step in the data processing was to reduce the data to a common coordinate system and resolution. For this we adopted the resolution of the NSO Fe XIV dataset, which has the lowest resolution in position angle of the five instruments.

For the MLSO data which were already in polar coordinates, all that needed to be done was to average together position angle bins to reduce the resolution from  $0.5^{\circ}$  to  $3^{\circ}$ , and average radially over an annulus approximately 70arcsec wide ( $\pm 35$ arcsec from the nominal radius).

Unlike MLSO where daily (*i.e.* 5 h) average images are available, LASCO data are only available as individual frames. Therefore to improve the signal to noise and also to make any time-smearing effects comparable to those in the MLSO data, we first read a full day of images and made exposure corrections by the method described by Tappin, Simnett and Lyons (1999). We then generated four 6-hour average images for each day.

Since LASCO uses a camera with a rectangular CCD rather than a rotating linear detector, the raw images are in cartesian coordinates. We therefore needed to convert the image to polar coordinates. To do this, the field of view was divided into radial bins of width equal to four pixels in the original data (47.6 arcsec for C2 and 224 arcsec for C3) and into  $3^{\circ}$  sectors in position angle. For each resulting cell, the pixels whose centres lie in the cell were determined and the count rates in those pixels were averaged.

We then selected a number of radii at which to extract circumferential profiles covering the range from  $1.15$  to  $2.35R_{\odot}$  for the MLSO data,  $2.5$  to  $4.0R_{\odot}$  for LASCO C2 and  $5$  to  $20R_{\odot}$  for LASCO C3. The full list of heights used is shown in Table 1. It should be noted that prior to July 1997, the majority of LASCO images were not full-

field. As a result the C2 scans above about  $3.5R_{\odot}$  and C3 scans above about  $18R_{\odot}$  have a lower signal-to-noise over the poles prior to that date.

Because the different position angles in the LASCO images were recorded with different parts of the detector, we found that variations in the detector dark current resulted in certain latitudes at which persistent maxima and minima occurred. Since these instrumental features make it difficult to see the maxima due to solar wind structures, it was necessary to find a way to remove them. We have found that an effective method is to divide the data into one year blocks so as to have a long enough base, but also to handle the variations in the CCD properties with time. For each year, we determine the fifth percentile of data at each location in the scans, and subtract the resulting value from all the scans for that year. This is chosen in preference to using an annual minimum as there are occasional corrupt images which are likely to dominate the minimum.

In 2004, the Z-axis drive of SOHO's high-gain antenna failed. Since that time the spacecraft has performed a  $180^{\circ}$  roll manoeuvre four times a year to keep Earth in the antenna beam. This was corrected after the CCD pattern removal to align the scans correctly.

For all the datasets we then followed Alrock (2003) and defined a significant maximum as one in which the brightness at a position angle was a local maximum, and also its immediate neighbours exceeded the next pair of position angles (*i.e.* for position angle index  $i$  to be considered a significant maximum then

$$b_{i-2} < b_{i-1} < b_i > b_{i+1} > b_{i+2} \quad (1)$$

must be satisfied;  $b_i$  denotes the observed intensity at position angle index  $i$ ). As well as excluding noise, this criterion also eliminates most maxima due to stars and planets (even Venus in LASCO C3 does not extend over  $15^{\circ}$ ). This method does not distinguish bright and faint maxima, but rather gives us a measure of where streamers are present. To adjust the observation dates of the two limbs to central meridian, maxima over the East limb were assigned a date seven days later than the date of observation, while those over the West limb were given a date seven days earlier. We then convert the position angles of the maxima to latitude (on the assumption that the features lie above the limb). For LASCO we excluded the quadrant containing the occulter support pylon as this region is vignetted by the pylon thus compromising our ability to detect maxima. The maxima for all four (or three for LASCO) quadrants were then combined to give a list of maxima against absolute latitude. We consider that the gain in signal to noise thus obtained outweighs any loss of information about North-South asymmetries (*c.f.* Alrock, 2011). All the quantitative fits presented in this paper are made by fitting to this list of maxima.

For the purposes of displaying the data we then counted the number of maxima that were detected in each latitude bin for each Bartels (27 day) rotation, and divided by the number of scans or images in the rotation to give a probability of a maximum at that latitude. To facilitate visualisation we smooth the counts of maxima using a nine rotation running mean, which was chosen as giving the best apparent balance between signal to noise and smearing.

## 4 Results

In Figure 1, we show the NSO green line activity map and two of those for the MLSO white light polarised brightness for the interval 1986 to 2011 (solar cycles 22 and 23). These maps show the number of maxima as a function of latitude and date. We remind the reader that this does not show the amplitude of the maxima, only the number. All three maps show a similar structure with two overlapping cycles drifting towards the equator, and also the rush to the poles. The most important feature to notice here is that the NSO map at  $1.15R_{\odot}$  and the MLSO map at the same height match very closely although the latter is considerably noisier. Since the K-coronal intensity is a function of density only, while the green line emission is a function of both density and temperature, the close match shows that the activity zones must be primarily density rather than temperature features. The MLSO map at  $2.35R_{\odot}$ , shows a similar structure to the maps at  $1.15R_{\odot}$ , but as can be seen by comparing it with the overlaid contour of the green line activity it is very clear that the movement of the activity towards the equator during the declining phase of both cycles is much faster than at  $1.15R_{\odot}$ .

For a more quantitative analysis of the variation of the latitude of the activity zones with height, we concentrate on the interval for which we also have LASCO data, namely 1996-2010 which corresponds to solar cycle 23. A selection of these datasets are shown in Figure 2.

It should be noted that the constant band of “activity” below  $20^{\circ}$  latitude in LASCO C3 is due to the F-corona which dominates at these altitudes. Even though the CCD irregularity removal does also reduce this contribution, the small changes in apparent width and inclination of the F-corona as the Earth orbits the Sun still produce a dominant contribution to the number of detected maxima. Unfortunately this means that we cannot track the activity bands below about  $20^{\circ}$  latitude in C3.

For the purposes of this study, we have considered only the interval from 2001 to the start of 2008, where (a) the equatorward drift is approximately linear in time and (b) it can be clearly seen in all the instruments at all heights (we therefore do not consider the abrupt acceleration of the drift from about the start of 2009, which is also the time at which the cycle 24 rush to the poles separated from the equatorward drift). To quantify the trend in the equatorward drift we firstly define manually a region which contains the activity band of the drift, this is done simply by examining the activity maps and drawing a box around the band of activity. We then perform a linear fit to all the recorded maxima within that region to obtain a slope and intercept. The chosen region and the comparison of the smoothed map and the individual maxima is shown in Figure 3. This method was chosen in preference to fitting to the maxima at each time (as was done by Altrock (2003) for seven-rotation averages) since it is less sensitive to spurious maxima. The fits thus derived are indicated in Figure 2 as dashed black and white lines.

It is clear from the activity zone maps in Figure 2 that at all heights, the coronal activity zones reach a maximum latitude of around  $75^{\circ}$  near solar maximum in 2000 and then the latitude of the activity zones moves toward the equator through the declining phase of the cycle. However the drift to the equator is clearly much faster at higher altitudes, and by about  $4R_{\odot}$  there is little if any overlap between the cycles. To show this more clearly, we overlay all the fitted trends from Figure 2 in Figure 4a.

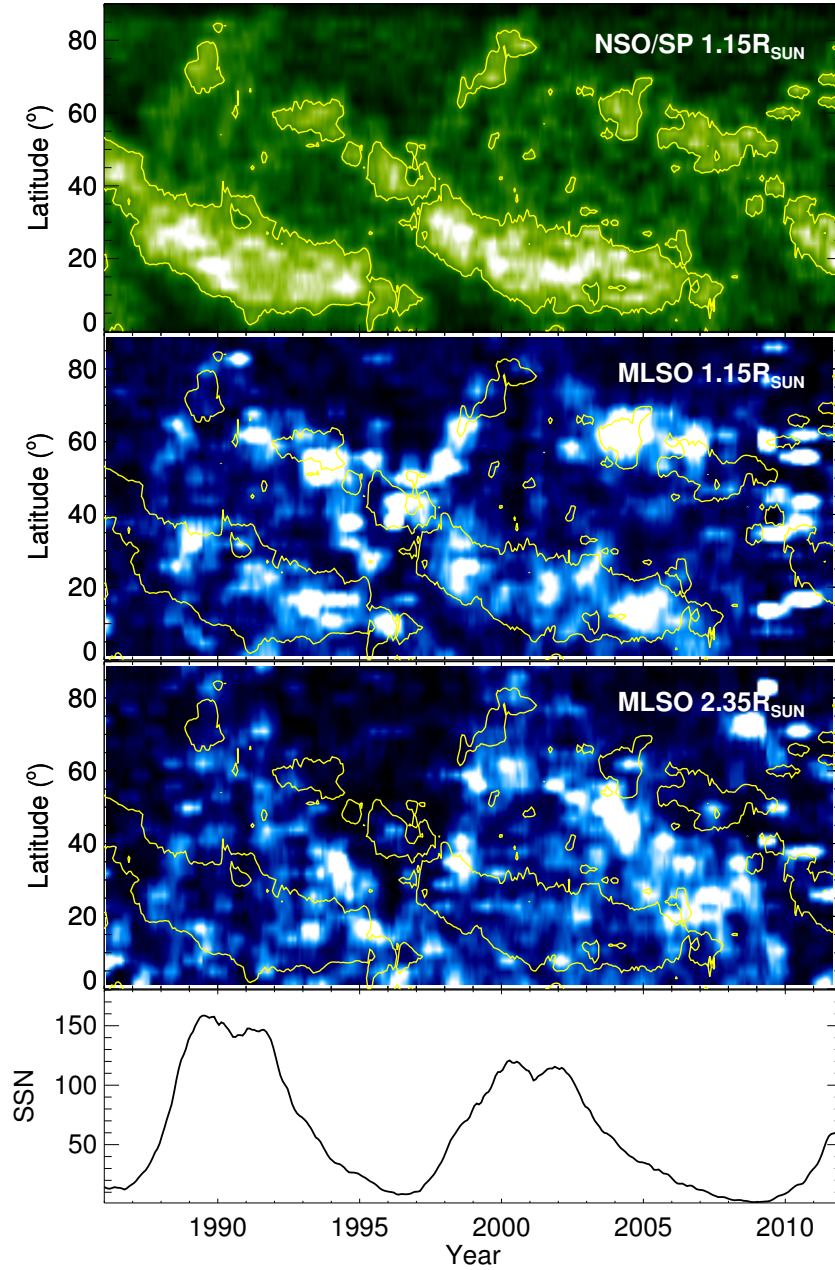


Figure 1: The evolution of the zones of activity from 1986 to 2012. The panels show (from top to bottom) the NSO green line data at  $1.15R_{\odot}$ , the MLSO white-light data at  $1.15R_{\odot}$ , the MLSO data at  $2.35R_{\odot}$ , and the smoothed sunspot number. A single contour of the NSO green line map is shown in yellow over each panel to facilitate comparison. N.B. all heights are measured from the centre of the Sun.

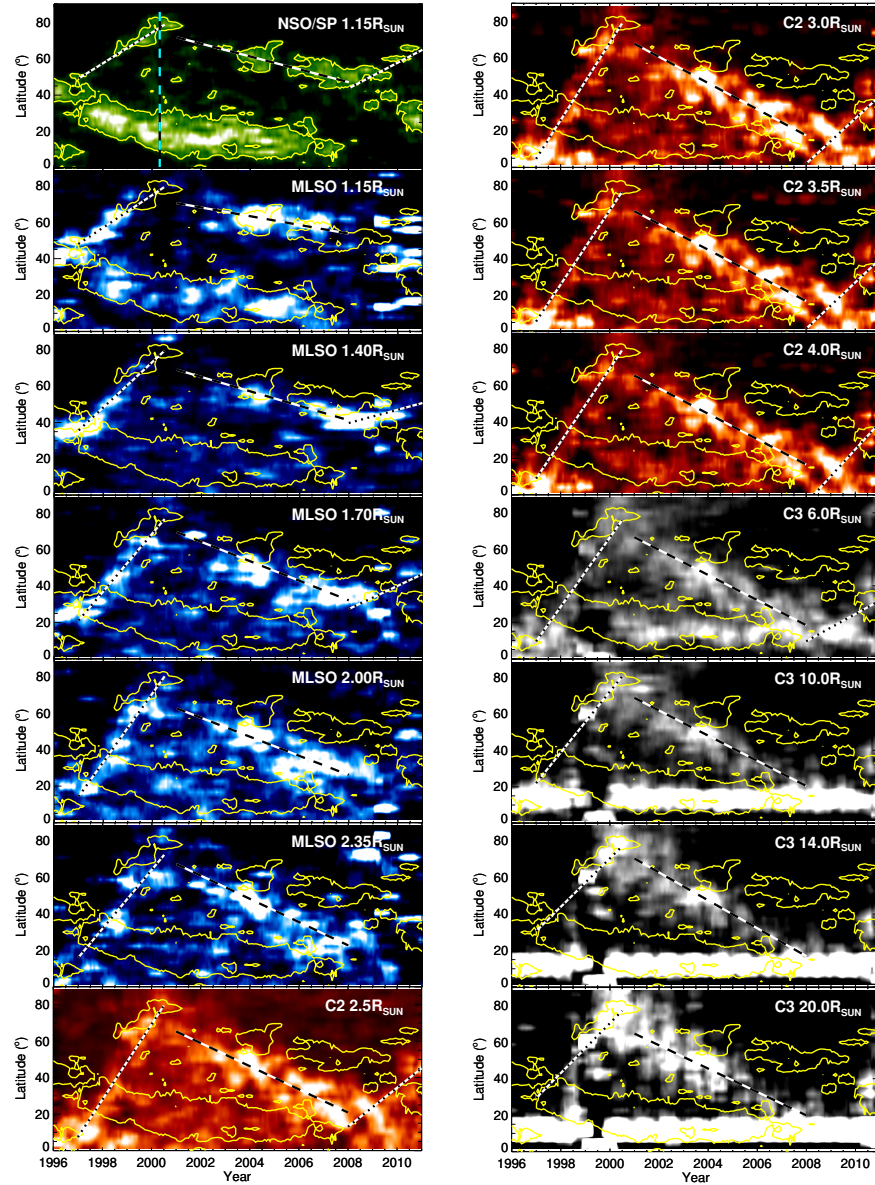


Figure 2: The evolution of the zones of activity for selected heights in the corona, from 1996 to 2011 (FeXIV in green, MLSO in blue, LASCO C2 in red, LASCO C3 in grey, respectively). For each height, a single contour from the NSO green line map (yellow) is superposed to facilitate comparison. Also superposed on each map is an estimate of the gradient of the drift towards the equator (black and white dashed lines), and of the “rush to the poles” (black and white dotted lines, black on white for cycle 23, white on black for cycle 24). The rush to the poles for cycle 24 is only shown for those heights at which it can be clearly discerned. The persistent maxima seen below  $20^\circ$  latitude in the LASCO C3 plots, the final four panels with heights of  $6R_\odot$  and above, is an effect of the F-corona which we have not been able to eliminate. The date of solar maximum is indicated by the cyan and black dashed line overlaid on the NSO map (upper left panel).

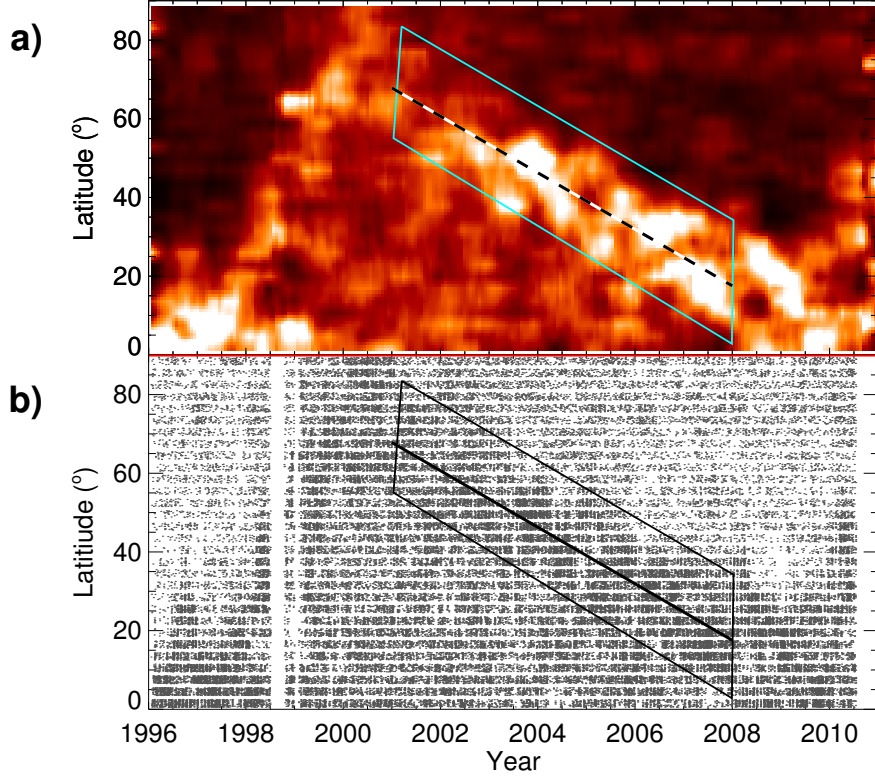


Figure 3: The process of fitting the trends to the drift. The example here is for LASCO C2 at  $3.0R_{\odot}$ . (a) The activity map and (b) The raw maxima (N.B. in the figure a random number between -1 and +1 is added to the latitude of each point to separate the individual points and allow the reader to see the variation of point density more easily). In each case the region of the equatorward drift is outlined with a medium weight box, and the fit is shown with a heavy line. The fit is generated by a linear regression to all the points within the region-of-interest box.



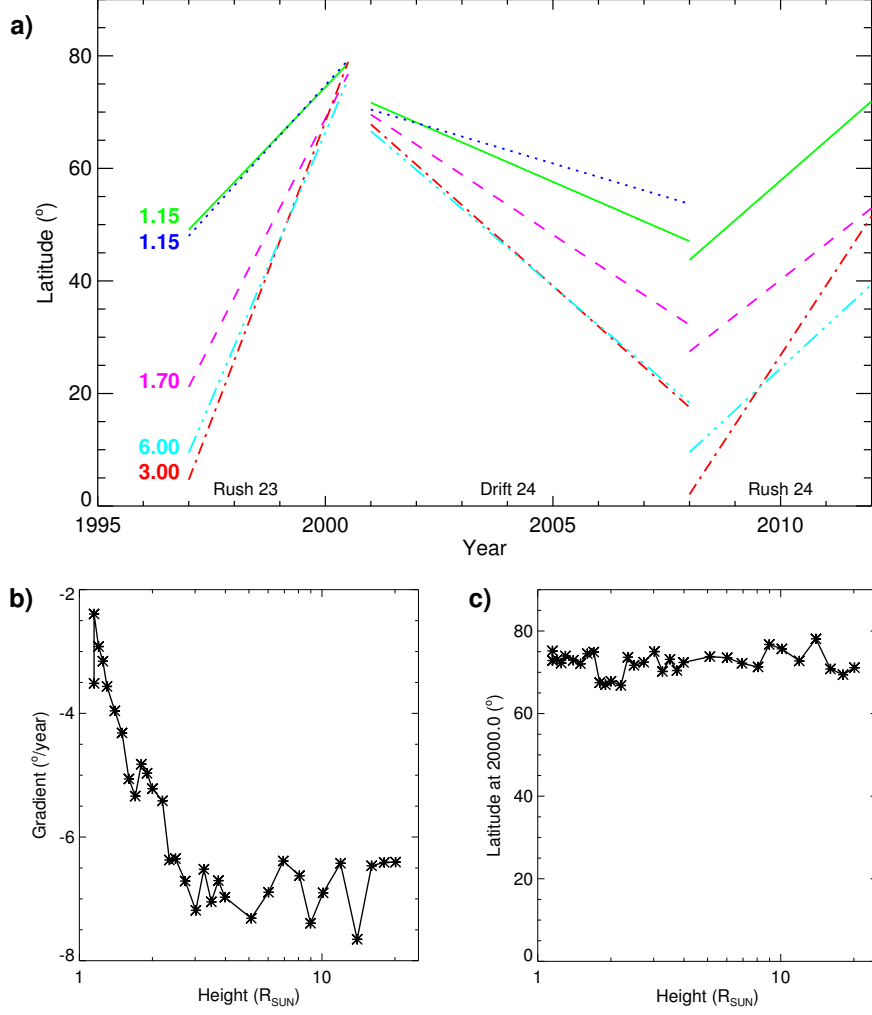


Figure 4: (a) The trends of selected equatorward drifts, and the rushes to the poles as overlayed on Figure 2. The heights are indicated to the left of the tracks for the cycle 23 rush to the poles, for the two trends at  $1.15R_{\odot}$ , the solid green lines are the NSO green-line data and the dotted blue lines are the MLSO data. Note that the rush of cycle 24 could not be discerned for the MLSO data at  $1.15R_{\odot}$ . (b) The variation of equatorward drift rate with height as determined from the slope estimates in Figure 2. (c) The variation of latitude of the start of the equatorward drift at 2000.0 with height.

We plot the gradients of the estimates of the drift to the equator in Figure 4b, along with the latitude at the start of 2000 in Figure 4c. This shows clearly that close to the Sun, the drift rate is around  $3^\circ/\text{year}$ , but that this increases to about  $7^\circ/\text{year}$  by  $3-4R_\odot$ , above that height the gradient is constant within the errors of measurement. There is no clear trend in the latitude at the start of 2000, with a value close to  $75^\circ$  at all heights. We do not consider that the slight fluctuations are significant.

We note that there are a number of epochs during which high activity is seen at all heights. Most notable of these features is the enhanced activity in late 2003 and early 2004. This combined with the smooth change of latitude with height provides good evidence that we are observing the same structures at all heights.

The other main component of the extended cycle, the so-called “rush to the poles” which begins soon after solar minimum and reaches its highest latitude near to solar maximum, is also clearly visible at all heights. Historically the rush to the poles has been tracked from about  $45^\circ$  latitude at solar minimum up to high latitudes at maximum (Waldemeier, 1964; Altrock, 1997). However we see that higher in the corona the rush starts at about the same time as it does in the green-line measurements, but it begins at much lower latitudes. The trend that is observed at the start of cycle 23 is that the rush started at all altitudes early in 1997 when it branched away from the previous equatorward drift, and intersected the start of the next equatorward drift at the start of 2000. As with the equatorward drift, we have indicated our estimates of the rush to the poles during the rising phase of cycle 23 with dotted black and white lines in Figure 2. The start of the rush to the poles of cycle 24 is also apparent in the green line and the LASCO C2 data for 2009 and 2010.

## 5 Discussion

The most obvious trend that we see as we track the zones of activity to higher altitudes is that the drift towards the equator becomes more rapid as we move higher into the corona.

Could this be an observational artifact caused by changes in the Thomson-scattering weighting functions? For this to be the case, it would be necessary that the Thomson weighting functions become narrower (in angle as seen from the Sun) as the closest approach of the line of sight to the Sun moves further from the Sun. In fact the reverse is the case as the electron density falls off faster than  $1/r^2$  close to the Sun (*e.g.* Allen, 1973). In addition, the MLSO data (heights below  $2.35R_\odot$ ) use polarised light which has a much narrower weighting function than unpolarised (*e.g.* Howard and Tappin, 2009). The emission-line weighting is generally narrower than the Thomson function at the same distance since the dependence of the emission is approximately proportional to  $N_e^{1.7}$  and peaks at a temperature of about  $1.8 \times 10^6 \text{K}$  (Mason, 1975; Guhathakurta *et al.*, 1992). We have verified this by some simple simulations of radial streamers. These show that such streamers can never appear at a lower projected latitude than their footpoint, and that except at very high footpoint latitudes (above about  $60^\circ$ ) they predominantly appear close to the footpoint latitude. If (as seems probable) we are looking at a band of activity reaching up to a particular latitude, then a wider scattering function will increase the sensitivity of the observations to structures well-away from

the sky plane. Since a radial streamer away from the sky plane will have an apparent latitude greater than its true latitude this would tend to make that activity appear to extend closer to the poles, which is the reverse of the trend that we see, thus confirming that it cannot be an artifact of the different observing techniques.

It is well-known that flows from coronal holes diverge (*e.g.* Whang, 1983; Falceta-Gonçalves and Jatenco-Pereira, 2005), and also that during the declining and minimum phase of the solar cycle the solar wind is well-represented as a two-part system with low-latitude slow wind from the streamer belt and high-latitude fast wind coming from the polar coronal holes (*e.g.* Phillips *et al.*, 1995). The behaviour of the equatorward drift may then be understood if we assume that the upper zone of activity lies on the boundary between the low latitude corona and the polar coronal holes (most probably streamers overlying the polar crown filaments). That boundary moves equatorward as the polar holes become larger during the decline of the solar cycle. The divergence of the flow from the holes also squeezes the streamers towards the equator at higher altitudes. When the polar hole is smaller and weaker near solar maximum, we expect that not only will the boundary be closer to the poles, but that there will also be less divergence. While the exact degree of divergence will depend on the speeds and densities of the flows in the coronal holes and the streamer belt, the degree of equatorward deflection which we see is consistent with that found in the MHD simulations of Whang (1983).

To better visualise the shape of the activity zones in latitude and radius, we made annual averages of the activity levels as a function of radius and latitude for the declining phase of cycle 23, these are shown in Figure 5. In this format the image is a representation of the average path of the streamers from close to the Sun, into the high corona. The deflection of the activity zones towards the equator with increasing height in the low corona is very evident, as is their more radial nature in the higher corona. It is also very clear that the amount of deflection increases as we approach solar minimum.

We also see that the feature corresponding to the low-latitude “current” cycle activity zone in the low corona cannot be traced above about  $3R_{\odot}$  after 2003. It is unclear whether the streamers overlying the main activity belt simply do not extend into the high corona or whether they deflect polewards and merge with the high-latitude zone. The latter is hinted by some years, notably 2006 and 2007, however the apparent band joining the low-latitude activity to the high-latitude is in the MLSO data which have significantly poorer quality than either the NSO green line data or the LASCO data.

We thus have two possible interpretations of the long-term structure of the coronal activity during the declining phase of the cycle. These are illustrated schematically in Figure 6. If the apparent connection of the two bands at about  $2R_{\odot}$  is an artifact, then the structure is as shown in Figure 6(a), where the streamers over the main activity zone are closed loops which do not extend above a few solar radii. If on the other hand the connection is real, then the structure must be as in Figure 6(b), and the streamers from the activity belt merge with those originating at higher latitudes. It is of interest to compare this with the interpretation of a coronal ray observed during a solar minimum eclipse shown in Figure 136 of Shklovskii (1965).

Irrespective of which interpretation of the topology is correct, it is evident that at higher altitudes ( $> 3R_{\odot}$ ) the streamer belt is predominantly rooted in the higher-latitude activity band closer to the Sun. Hence we must expect that the slow solar wind

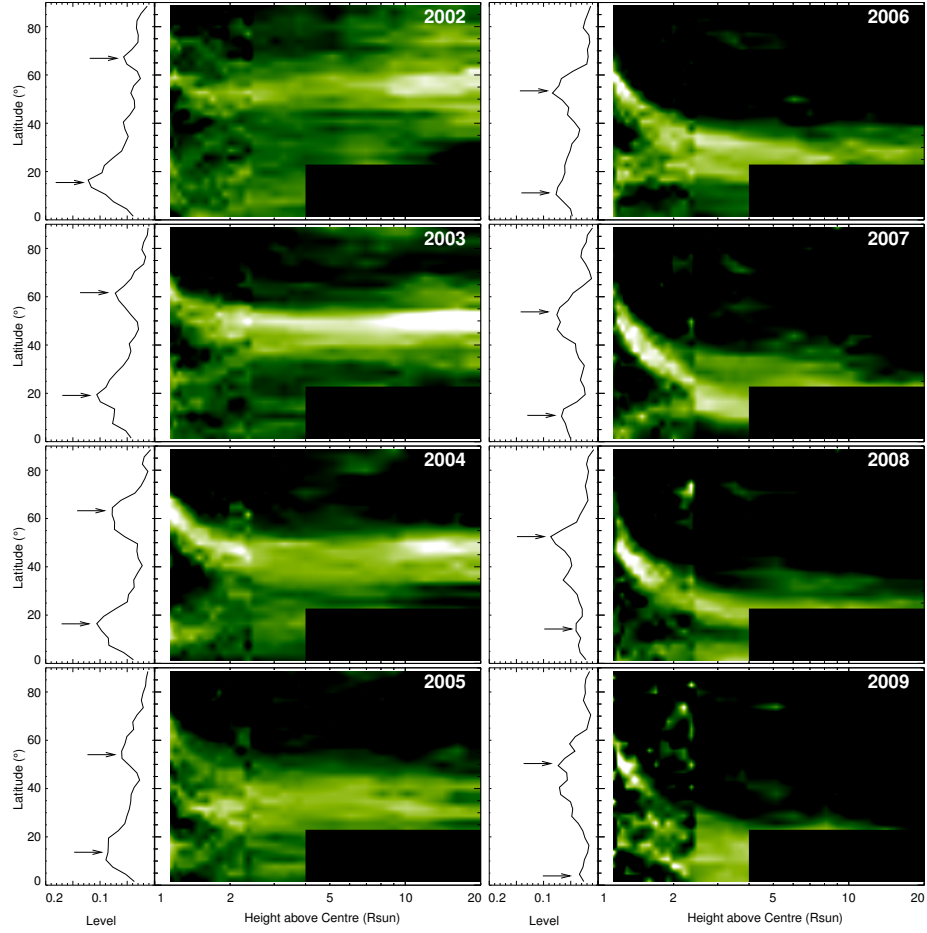


Figure 5: Annual averages of the activity distribution in the K-corona for the declining phase of cycle 23. The green line activity profile is plotted to the left of each year. The approximate latitudes of the two bands of activity are marked by the arrows on the green line profiles. LASCO C3 data below  $20^\circ$  latitude are omitted as these reflect the F-corona rather than the K-corona. For 2009, the low altitude data from MLSO are noisy as there were many data gaps during that year.

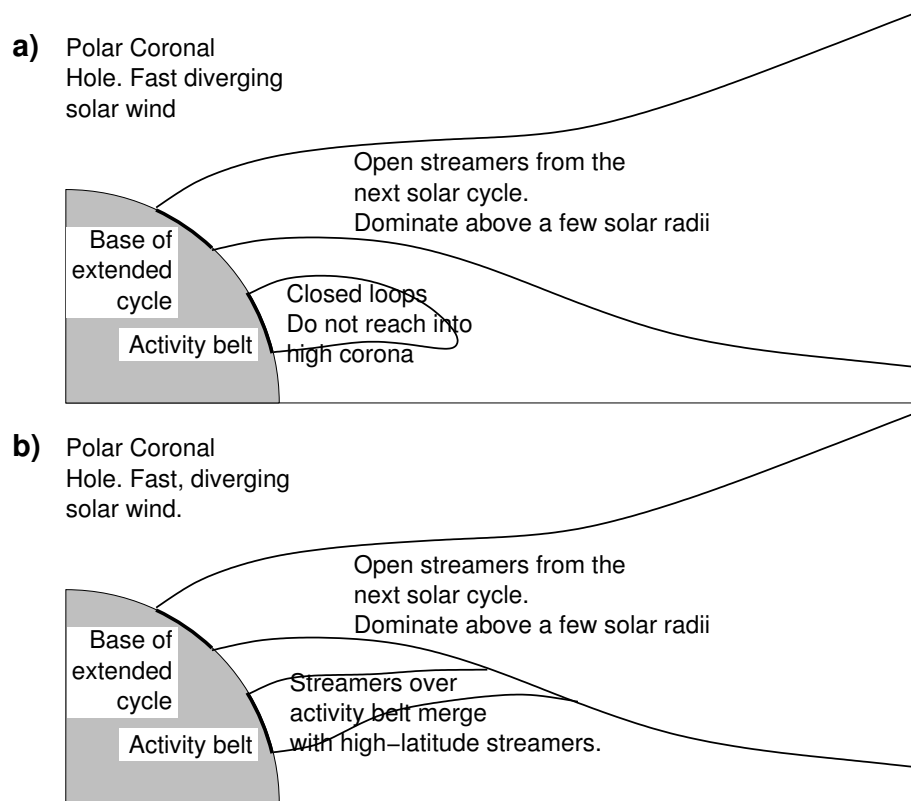


Figure 6: Schematic illustration of two possible interpretations of the streamer structure in the late declining phase of the solar cycle. (a) The streamers over the main activity belt are closed loops and do not extend above a few  $R_{\odot}$ , (b) The activity belt streamers merge with the high-latitude streamers.

seen by *in-situ* observations near Earth during the declining phase of the solar cycle, and especially after the lower edge of the equatorward drift reaches the equator (around 2007 for cycle 23), will include material characteristic of the next solar cycle.

We conjecture that the high-latitude streamers are those originating over the polar crown filaments, while the low-latitude ones originate above active regions. If this is the case then it is to be expected that as activity declines to solar minimum the importance of streamers from the active regions will decrease relative to those from the polar crown. However a full understanding of this would require a detailed study of the rising phase of the solar cycle, including photospheric and chromospheric observations to show how the polar-crown region transitions to the activity-belt region.

As with the equatorward drift, we find that the highest latitudes of the rush to the poles is similar at all heights. However at the start of the rush, it is at much lower latitudes at higher altitudes. It branches away from the equatorward drift at similar times at all altitudes. This may be explained in the same way as the latitudinal variation of the equatorward drift with altitude. That is, the polar coronal hole shrinks during the rise in activity, and so the boundary between the polar hole region and the polar crown region moves poleward and the flows from the polar hole become weaker. Thus as the rush move poleward its equatorward deflection decreases.

It is also evident from Figure 4a that for those heights at which we were able to determine the rush to the poles for cycle 24, it was taking place more slowly than at the corresponding heights in cycle 23. However the uncertainties in the determination of the rush for cycle 24 are large, and it is not clear that this is actually saying anything other than that the time between the maximum of cycle 23 and that of cycle 24 is longer than the interval in cycles 22 and 23.

## 6 Conclusions

We have shown that the activity zones of the extended solar cycle seen in the emission corona at  $1.15R_{\odot}$  can be traced far out into the corona in the Thomson-scattered light of the K-corona. We find that the activity zones are deflected towards the equator at greater heights in the corona. We also see that as the activity moves toward the equator through the declining phase of the cycle, the amount of deflection increases. This is consistent with the expansion of the flows from the polar coronal holes. This deflection also seen in the rush to the poles during the rising phase of the cycle.

During the declining phase of the solar cycle, the activity zones above a few solar radii are dominated by structure which connect to the high-latitude branch in the green-line activity, which is related to the upcoming solar cycle. It therefore seems inevitable that at least in the late declining phase of the solar cycle the low-latitude slow solar wind is more characteristic of the upcoming cycle than of the current. This opens up the possibility of determining some characteristics of the next cycle from *in-situ* measurements made well before the start of that cycle. In the case of the current cycle, it appears that cycle 24 should dominate from about 2007.

## acknowledgements

The Mauna Loa coronameter data are provided courtesy of the Mauna Loa Solar Observatory, operated by the High Altitude Observatory, as part of the National Center for Atmospheric Research (NCAR). NCAR is supported by the National Science Foundation. LASCO was built by a consortium of the Naval Research Laboratory (Washington, USA), the Max-Planck-Institut für Aeronomie (Lindau, Germany) the Laboratoire d'Astronomie Spatiale (Marseille, France) and the University of Birmingham (Birmingham, UK) and is a part of the SOHO mission which is a collaborative mission of ESA and NASA. Partial support for NSO (including the work of SJT and the operation of the coronagraph) is provided by the US Air Force under a Memorandum of Agreement.

## References

- Allen, C. W.: 1973, *Astrophysical Quantities*, Athlone Press, London, p176.
- Altrock, R. C.: 1997, *Solar Phys.* **170**, 411.
- Altrock, R. C.: 2003, *Solar Phys.* **216**, 343.
- Altrock, R. C.: 2011, *Solar Phys.* **274**, 251.
- Brueckner, G. E., Howard, R. A., Koomen, M. J., Korendyke, C. M., Michels, D. J., Moses, J. D., *et al.*: 1995, *Solar Phys.* **162**, 357.
- Elmore, D. F., Burkepile, J. T., Darnell, J. A., Lecinski, A. R., Stanger, A. L.: 2003, In: Fineschi, S. (ed), *Polarimetry in Astronomy, Proc. SPIE* **4843** 66.
- Falceta-Gonçalves, D. and Jatenco-Pereira, V.: 2005, In Gouveia Dal, E. M., Pino, G. L., Lazarian, A. (eds.), *Magnetic Fields in the Universe: From Laboratory and Star to Primordial Structures, AIP Conf. Proc.* **784** 591.
- Fisher, R. R., Lee, R. H., MacQueen, R. M., Poland, A. I.: 1981, *Appl. Opt.* **20**, 6.
- Guhathakurta, M., Rottman, G. J., Fisher, R. R., Orrall, F. Q., Altrock, R. C.: 1992, *Astrophys. J.* **388**, 633.
- Howard, T. A., Tappin, S. J.: 2009, *Space Sci. Rev.* **147**, 31.
- Labonte, B. J., Howard, R.: 1982, *Solar Phys.* **75**, 161.
- Mason, H. E.: 1975, *Mon. Not. Roy. Astron. Soc.* **170** 651.
- Phillips, J. L., Bame, S. J., Barnes, A., Barraclough, B. L., Feldman, W. C., Goldstein, B. E., *et al.*: 1995, *Geophys. Res. Lett.* **22**, 3301.
- Shklovskii, I. S.: 1965, *Physics of the Solar Corona, 2nd edition*, Pergamon Press, Oxford, p404.
- Tappin, S. J., Simnett, G. M., Lyons, M. A.: 1999, *Astron. Astrophys.* **350**, 302.

Waldemeier, M.: 1964, *Z. Astrophys.* **59**, 205.

Whang, Y. C.: 1983, *Solar Phys.* **88**, 343.

Wilson, P. R., Altrock, R. C., Harvey, K. L., Martin, S. F., Snodgrass, H. B.: 1988, *Nature* **333**, 748.